Substrate Specificity of the Human Protein Phosphatase 2Cδ, Wip1†

Hiroshi Yamaguchi,‡ Giuseppina Minopoli,‡ Oleg N. Demidov,‡ Deb K. Chatterjee,§ Carl W. Anderson,|| Stewart R. Durell,⊥ and Ettore Appella*,‡

Laboratory of Cell Biology and Laboratory of Experimental and Computational Biology, National Cancer Institute, National Institutes of Health, Bethesda, Maryland 20892, Protein Expression Laboratory, SAIC-Frederick, Inc., National Cancer Institute at Frederick, Frederick, Maryland 21702, and Biology Department, Brookhaven National Laboratory, Upton, New York 11973

Received November 2, 2004; Revised Manuscript Received January 20, 2005

ABSTRACT: Wip1, the *w*ild-type p53-*i*nduced *p*hosphatase, selectively dephosphorylates a threonine residue on p38 MAPK and mediates a negative feedback loop of the p38 MAPK-p53 signaling pathway. To identify the substrate specificity of Wip1, we prepared a recombinant human Wip1 catalytic domain (rWip1) and measured kinetic parameters for phosphopeptides containing the dephosphorylation sites in p38α and in a new substrate, UNG2. rWip1 showed properties that were comparable to those of PP2Cα or full-length Wip1 in terms of affinity for Mg^{2+}, insensitivity to okadaic acid, and threonine dephosphorylation. The substrate specificity constant k_{cat}/K_m for a diphosphorylated peptide with a pTXpY sequence was 6−8-fold higher than that of a monophosphorylated peptide with a pTXY sequence, while PP2Cα showed a preference for monophosphorylated peptides. Although individual side chains before and after the pTXpY sequence of the substrate did not have a significant effect on rWip1 activity, a chain length of at least five residues, including the pTXpY sequence, was important for substrate recognition by rWip1. Moreover, the X residue in the pTXpY sequence affected affinity for rWip1 and correlated with selectivity for MAPKs. These findings suggest that substrate recognition by Wip1 is centered toward a very narrow region around the pTXpY sequence. Three-dimension homology models of Wip1 with bound substrate peptides were constructed, and site-directed mutagenesis was performed to confirm the importance of specific residues for substrate recognition. The results of our study should be useful for predicting new physiological substrates and for designing specific Wip1 inhibitors.

Protein phosphorylation plays a crucial role in the regulation of many fundamental cellular processes, including the cell cycle, metabolism, and signal transduction. Phosphorylation levels are controlled by the opposing actions of kinases and phosphatases. Protein phosphatase 2C (PP2C)[1] is a member of the magnesium-dependent, serine/threonine protein phosphatase (PPM) family (*1*), which is characterized by dependence on Mg^{2+} for activity and by insensitivity to okadaic acid (OA), a potent inhibitor of PP1 or PP2A serine/threonine protein phosphatases (*2*, *3*).

The PP2C family negatively regulates mitogen-activated protein kinases (MAPK) that control cellular pathways for proliferation, differentiation, development of inflammatory response, and apoptosis (*4*). MAPKs are activated by phosphorylation of conserved threonine and tyrosine residues in their pTXpY motifs by activated MAPK kinases (MAPKK). MAPKKs, in turn, are activated by phosphorylation of the conserved serine/threonine residues in their pSXXX(pS/pT) motifs by MAPKK kinases (MAPKKK). PP2Cα and PP2Cβ, members of the PP2C family, directly dephosphorylate the serine/threonine residues of these motifs in p38 MAPK and in MKK3, MKK4, MKK6, and MKK7 MAPKKs to inactivate p38 and c-Jun N-terminal kinase (JNK) regulated pathways involved in stress responses (*5*, *6*). PP2C has been shown to similarly regulate MAPK pathways in yeast (*7*−*9*) and plants (*10*), indicating that the PP2C family plays an important role in many organisms.

Wip1 (PPM1D or PP2Cδ) is a member of the PP2C family and was identified as a wild-type p53-induced phosphatase that accumulates after DNA damage (*11*). Like other PP2C family members, Wip1 specifically inactivates p38 MAPK through dephosphorylation of threonine in its pTGpY sequence (*12*). Phosphorylated p38 MAPK activates p53 to cause cell cycle arrest and apoptosis in response to DNA damage (*13*−*15*); thus, Wip1 mediates a feedback regulation of the p38 MAPK signaling pathway that negatively regulates p53 function (*12*). We recently reported that Wip1 interacts with a nuclear isoform of uracil DNA glycosylase (UNG2)

† D.K.C. was supported in whole or in part with Federal funds from NCI, NIH, under Contract N01-CO-12400. C.W.A. was supported in part by a Laboratory Directed Research and Development Award at the Brookhaven National Laboratory under contract with the U.S. Department of Energy.

* To whom correspondence should be addressed. Tel: 301-402-4177. Fax: 301-496-7220. E-mail: appellae@pop.nci.nih.gov.

‡ Laboratory of Cell Biology, National Cancer Institute.

§ Protein Expression Laboratory, SAIC-Frederick, Inc.

|| Biology Department, Brookhaven National Laboratory.

⊥ Laboratory of Experimental and Computational Biology, National Cancer Institute.

[1] Abbreviations: ERK, extracellular signal-regulated kinase; Fmoc, 9-fluorenylmethoxycarbonyl; GST, glutathione *S*-transferase; IPTG, isopropyl 1-thio-β-D-galactopyranoside; JNK, c-Jun N-terminal kinase; MAPK, mitogen-activated protein kinase; MAPKK, MAPK kinase; MAPKKK, MAPKK kinase; OA, okadaic acid; PPM, protein phosphatase magnesium dependence; PP2C, protein phosphatase 2C; pX, phosphorylated amino acid; UNG2, nuclear uracil DNA glycosylase; Wip1, wild-type p53-induced phosphatase.

10.1021/bi0476634 CCC: $30.25
Published on Web 03/12/2005

and suppresses base excision repair through threonine dephosphorylation on its pTLpY sequence (*16*). We therefore suggested that this process of Wip1-mediated dephosphorylation is part of a wider negative feedback regulation loop initiated by p53 (*16*). Recent studies have shown that the gene for Wip1, *PPM1D*, is amplified or overexpressed in several human tumor types and acts as an oncogene (*17*−*20*). We also showed that disruption of *PPM1D* activates not only p53 but also the $p16^{INK4a}$−$p19^{ARF}$ pathways through p38 MAPK signaling (*21*). These studies suggest that inhibition of the Wip1 gene or protein may be a good strategy for treating certain types of cancer (*21*, *22*).

Studies using *PPM1D* null mice indicate that Wip1 has an important role in spermatogenesis, lymphoid cell function, and cell cycle regulation (*23*). However, the only physiological substrates identified to this point are p38 MAPK and UNG2. Understanding Wip1 substrate specificity should not only help to predict other physiological substrates but may also be useful in the design of specific inhibitors. In this study, we investigated the substrate specificity of Wip1 using its recombinant catalytic domain (residues 1−420 in human) and phosphopeptides that contained sites from p38α MAPK and UNG2 that Wip1 dephosphorylates. The kinetics of these reactions were compared with computer simulations of docking of the same peptides to help to identify the unique structural determinants that distinguish the substrate specificities of the PP2Cα and Wip1 enzymes.

EXPERIMENTAL PROCEDURES

Expression and Purification of the Human Wip1 Catalytic Domain (rWip1) and Its Mutants. The wild-type Wip1 cDNA (bases 1−1250) was cloned into the *Bam*HI−*Not*I sites of the pET-23a vector (Novagen) by PCR using the following oligonucleotide primers: 5′-taaggatccATGGGTTCTCATCATCATCATCATCATGGTatggcggggctgtactcgct-3′ (forward, containing the nucleotides codifying the 6× His tag at the 5′ end) and 5′-ccgaaagcggccgcATTACTTGACTGGTGGTGTAGAACATGG-3′ (reverse). The fragment containing the T7 tag carried by the vector was eliminated by digestion with *Nde*I and *Bam*HI followed by ligation of the filled extremities.

The resulting plasmid, pET-23a-Wip1 (1−1250), was used to transform *Escherichia coli* BL21(DE3). Transformed bacteria were grown on LB/ampicillin (100 μg/mL) plates. A single colony was selected and grown in 10 mL of LB broth containing 100 μg/mL ampicillin overnight with shaking at room temperature. The culture was transferred to 1 L of LB broth containing 50 μg/mL ampicillin and shaken at room temperature until the absorbance at 600 nm was between 0.6 and 0.7. Following the addition of isopropyl 1-thio-β-D-galactopyranoside (IPTG) to a final concentration of 0.02 mM, the culture was incubated at 15 °C with shaking for 20 h. The cells were harvested by centrifugation at 4000 rpm at 4 °C for 10 min, and the cell pellets were resuspended in 10 mL of PBS with EDTA-free protease inhibitor cocktail tablets (Roche, Indianapolis, IN), 2 mM 2-mercaptoethanol, and 0.2% Triton X-100 and then lysed by sonication. The cell debris was removed by centrifugation at 10000 rpm for 40 min at 4 °C, and the supernatant was decanted into a 50 mL conical tube to which 2 mL of a 50% slurry of TALON metal affinity resin (Clontech, Palo Alto, CA) equilibrated with PBS was added. After incubation with gentle agitation at 4 °C for 1 h, the resin was transferred to a column and washed with 5 mM imidazole in washing buffer (PBS, 500 mM NaCl, 10% glycerol, 0.2% ethanol, 1 mM 2-mercaptoethanol). The N-terminal histidine-tagged rWip1 was eluted by addition of five bed volumes of 150 mM imidazole in washing buffer. The eluents were concentrated with a Microcon YM-10 unit (Millipore, Bedford, MA) and dialyzed against phosphatase buffer (50 mM Tris-HCl, pH 7.5, 0.1 mM EGTA, 0.02% 2-mercaptoethanol).

The point mutations of rWip1 were generated by using the QuickChange protocol as described by the manufacturer (Stratagene, La Jolla, CA). The sequences of the oligonucleotides used for K238Q were 5′-GGACTTGGTGGGAGTGTAATGAACCAGTCCGGAGTGAATCGTGTAGTTTGGAAACGAC-3′ and 5′-GTCGTTTCCAAACTACACGATTCACTCCGGACTGGTTCATTACACTCCCACCAAGTCC-3′. A *Bsp*EI site was created in the oligonucleotides (underlined) without changing any amino acid for easy screening of mutant clones. The oligonucleotides used for the K238D mutation were 5′-GGACTTGGTGGGAGTGTAATGAACGATTCCGGAGTGAATCGTGTAGTTTGGAAACGAC-3′ and 5′-GTCGTTTCCAAACTACACGATTCACTCCGGAATCGTTCATTACACTCCCACCAAGTCC-3′. As before, a *Bsp*EI site (underlined) was created in the resulting mutant clone. Mutant R110E was created by the same procedure using the following oligonucleotides: 5′-CTTTTTCGCCGTGTGCGACGGCCATGGCGGGGAGGAGGCGGCACAGTTTGCCCGGGAGC-3′ and 5′-GCTCCCGGGCAAACTGTGCCGCCTCCTCCCCGCCATGGCCGTCGCACACGGCGAAAAAG-3′. In this case a *Nco*I site (underlined) was introduced in the oligonucleotide without changing any amino acids. Following PCR, the PCR products were digested with *Dpn*I to eliminate parental plasmid. Finally, the *Dpn*I digested products were used to transform DH5α. Colonies were selected on ampicillin-containing plates (100 μg/mL), and mutants were screened for the presence of the respective restriction enzyme sites. Finally, all mutants were sequenced to confirm the mutations.

Mutant plasmids were cotransformed with pACYC-Duet (Novagen) expressing Skp and DsbC (unpublished) proteins into BL21 cells (Invitrogen, Carlsbad, CA). Transformed colonies were selected on plates containing ampicillin (100 μg/mL) and chloramphenicol (15 μg/mL). Cultures (800 mL) were grown to mid log phase in Circle Grow (Q-Biogen, Irvine, CA) at 37 °C before transfer to a 16 °C incubator. After incubation for approximately 15 min, cells were induced with 0.75 mM IPTG for 16 h. Cultures were harvested and purified as described above. The purified protein was stored at −80 °C until use. Other recombinant proteins were purchased from Upstate Biotechnology (Charlottesville, VA).

Peptide Synthesis. Peptides were synthesized by the solid-phase method with Fmoc (9-fluorenylmethoxycarbonyl) chemistry. Phosphoamino acids were incorporated as Fmoc-Thr[PO(OBzl)OH]-OH, Fmoc-Ser[PO(OBzl)OH]-OH, and Fmoc-Tyr(PO_3H_2)-OH (Novabiochem, San Diego, CA). Acetylation of the N-terminus was achieved with acetic anhydride in the presence of 4-methylmorpholine. The peptides were purified by high-performance liquid chromatography on a Vydac C-4 column with 0.05% trifluoroacetic acid/water/acetonitrile. The masses of the peptides were

confirmed by matrix-assisted laser desorption ionization time-of-flight mass spectrometry (Micromass, Beverly, MA).

Steady-State Kinetic Assay. Phosphatase activity was measured by a malachite green/molybdate-based assay (*24*−*26*) following protocols provided by the manufacturer (serine/threonine phosphatase assay; Upstate Biotechnology). The amount of phosphate released was calculated using a phosphate standard curve. All assays were carried out in phosphatase buffer (50 mM Tris-HCl, pH 7.5, 0.1 mM EGTA, 0.02% 2-mercaptoethanol) by incubation with phosphopeptide and 30 mM $MgCl_2$ for 5−10 min at 30 °C. Under these conditions, 2-mercaptoethanol does not affect the development of dye color, and the phosphopeptide was dephosphorylated by less than 15%. To determine the kinetic parameters K_m and k_{cat}, the initial velocities (v) were measured at various peptide concentrations ([S]), and data were fitted to the Michaelis−Menten equation (eq 1).

$$v = k_{cat}[S]/(K_m + [S]) \quad (1)$$

For the Mg^{2+} concentration-dependence assay, reactions were carried out in phosphatase buffer containing 50 μM human p38α(175−185)(180pT 182pY) diphosphorylated peptide containing phosphothreonine 180 and phosphotyrosine 182 and various concentrations of Mg^{2+} for 5 min at 30 °C. The kinetic parameters were estimated by eq 1.

Immunoblotting. The phosphorylated, full-length p38α-GST fusion protein (600 ng) was reacted with rWip1 or recombinant human PP2Cα (100 ng) in phosphatase buffer containing 30 mM $MgCl_2$ at 30 °C for 30 min. Reactions were terminated by adding 2× SDS−PAGE sample buffer. The proteins were resolved by SDS−PAGE and transferred to PVDF membranes. After being blocked with 4% BSA, membranes were probed with anti-phospho-p38 polyclonal antibody (Thr180/Tyr182; Cell Signaling Technology, Beverly, MA), anti-phospho-Tyr monoclonal antibody (P-Tyr-102; Cell Signaling Technology), or anti-GST monoclonal antibody (B-12; Santa Cruz Biotechnology Inc., Santa Cruz, CA) and were detected using appropriate peroxidase-conjugated secondary antibodies (Amersham Bioscience, Piscataway, NJ) and ECL detection (Amersham Bioscience).

Dephosphorylation of Recombinant p38α Phosphoprotein by Phosphatases. The phosphorylated, full-length p38α-GST fusion protein (1.0 μM) was reacted with rWip1 (0.4 μM) in phosphatase buffer containing 50 mM $MgCl_2$ at 30 °C for up to 50 min. Aliquots were withdrawn at the indicated times, and the reaction was terminated by adding 2× SDS−PAGE sample buffer. Samples were subjected to immunoblotting analysis using anti-phospho-p38 antibody as described above. Changes in the phosphorylation state of the p38 proteins were quantified by densitometry. The data were fitted to the integrated Michaelis−Menten equation (eq 2) (*27*, *28*) to obtain the apparent k_{cat}/K_m:

$$t = p/k_{cat}E_0 + (K_m/k_{cat}E_0)\ln(p_\infty/p_\infty - p) \quad (2)$$

where E_0 is the enzyme concentration and p and p_∞ are the product concentrations at time t and infinity, respectively.

Structural Analysis. Protein sequences homologous to human Wip1 were obtained by searching the Swiss-Prot Protein Knowledgebase (*29*). Since the focus was on human Wip1 and PP2Cα, the list was trimmed to include only the α, β, γ, and δ subfamilies of the PP2C family from mammalian species. These included the α, β, and γ subfamilies found in humans, mice, and cattle and the δ members (i.e., Wip1) found in humans and mice. To study the patterns of residue conservation, a multisequence alignment was constructed using the ClustalX computer program (*30*). For regions of individual sequences not firmly aligned by obvious homology, manual editing was done to align residues known to be important in the active site (see text). The homology model of Wip1 was produced manually with the Swiss-PdbViewer computer program (*31*) using the above-mentioned multisequence alignment and the crystal structure of human PP2Cα (*32*) as a template. Little attention was given to correctly predicting the conformation at regions of insertions or deletions, since these were all found to be relatively distant from the active site that was of primary interest.

Simulations of the docking of p38 peptide substrate (DEMpTGpYVA) to the Wip1 and PP2Cα enzymes were performed with the AutoDock 3 computer program package (*33*). The atomic coordinates of the diphosphorylated peptides were generated and minimized with the CHARMM computer program (*34*). For the docking simulations, the two metal ions of the enzymes were treated as magnesiums, using the supplied van der Waals parameters and assigning electrostatic charges of +2e. Each phosphate of the substrate was given a charge of −2e. Simulations were started with the substrate peptides in an extended conformation, either randomly positioned in the grid or with the phosphate of the threonine residue in approximately the same position as the phosphate ligand in the catalytic site of the PP2Cα crystal structure (*32*). In the latter case, the peptide chain was given one of two opposite orientations along the cleft of the active site. At least 100 simulations were run for each of the peptides binding to each of the enzymes, with each of the three starting states. The dockings were carried out according to the Larmarckian genetic algorithm with a population size of 200 and the maximum number of generations and energy evaluations set to 1×10^5 and 5×10^6, respectively. The default values were used for all other runtime parameters. To modulate flexibility of the substrate, the nonamide bonds of the peptide backbone and the single bonds of the side chains were allowed to rotate freely.

RESULTS

The Activity of the Wip1 Catalytic Domain (rWip1) Is Comparable to That of PP2Cα or Full-length Wip1. The N-terminally His-tagged human Wip1 catalytic domain (residues 1−420), rWip1, was expressed in *E. coli* and was purified by metal affinity chromatography. The purity of rWip1 was more than 90% as determined by SDS−PAGE and Coomassie staining (data not shown).

The PP2C family, including Wip1, is insensitive to OA and is dependent on Mg^{2+} for phosphatase activity (*3*, *11*, *24*, *35*). To confirm the catalytic properties of rWip1, its phosphatase activity was determined using the human p38α-(175−185)(180pT 182pY) diphosphorylated peptide as a substrate. As shown in Figure 1A, the phosphatase activity of rWip1 is dependent on Mg^{2+}. One hundred nanomolar OA, which inhibited the PP1 and PP2A protein phosphatases (*36*), did not affect the activity of rWip1 (data not shown),

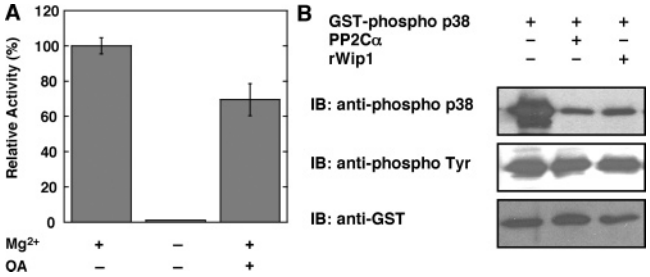

FIGURE 1: Characterization of rWip1 as a PP2C phosphatase. (A) Effects of Mg^{2+} and okadaic acid (OA) on rWip1 phosphatase activity measured with a p38α(175−185)(180pT 182pY) diphosphorylated peptide. The concentrations of the peptide, Mg^{2+}, and OA were 50 μM, 30 mM, and 20 μM, respectively. (B) Immunoblot analysis of rWip1 or PP2Cα-catalyzed dephosphorylation of the full-length p38α(180pT 182pY) GST-tagged phosphoprotein. The phosphorylation states of GST-tagged p38α(180pT 182pY) were analyzed with an anti-phospho-p38 (top panel) antibody that recognizes the diphosphorylation at Thr180 and Tyr182 of p38 or with an anti-phospho-Tyr (middle panel) antibody. The GST-tagged p38α protein level of each reaction was confirmed with an anti-GST (bottom panel) antibody. The graph shows the mean ± standard error of at least three experiments. All assays were performed at 30 °C and pH 7.5.

although at high concentrations of OA (20 μM), the activity of rWip1 was partially inhibited (~30%), a result that indicates rWip1 is insensitive to OA. Immunoblot analysis (Figure 1B) of rWip1-catalyzed dephosphorylation of the full-length p38α(180pT 182pY)-GST phosphoprotein showed that rWip1 removed only the phosphothreonine as previously reported (*12*). To further confirm the threonine-specific dephosphorylation, the absorbance at 282 nm of the p38α-(175−185)(180pT 182pY) diphosphorylated peptide was measured. This assay is based on the marked differences in the absorbance coefficient at 282 nm between phosphotyrosine and tyrosine (*27*). No absorbance change following incubation with or without rWip1 was observed (data not shown), indicating that the phosphotyrosine was not dephosphorylated by rWip1. Threonine-specific dephosphorylation of GST-p38α and the p38α diphosphorylated peptide also was observed after incubation with PP2Cα as reported (*5*). These results indicate that rWip1 has the phosphatase properties of the PP2C family, and these properties are comparable to those of the full-length Wip1 (*11*, *12*).

Magnesium Ion Is a Pseudosubstrate for rWip1. A kinetics analysis of PP2Cα indicated that the concentration of metal ions, such as Mg^{2+}, obeys Michaelis−Menten saturation kinetics, suggesting that metal ions act as pseudosubstrates (*24*). To determine whether rWip1 has the same property, the kinetic parameters K_m and k_{cat} were determined for different Mg^{2+} concentrations at a constant concentration of the p38α(175−185)(180pT 182pY) diphosphorylated peptide. A typical set of initial velocities versus Mg^{2+} concentrations is shown in Figure 2A. As for PP2Cα, Mg^{2+} also behaves as a pseudosubstrate for rWip1. Direct curve fitting of the data to the Michaelis−Menten equation yielded k_{cat} and K_m, which were 1.9 ± 0.1 s^{-1} and 8 ± 1 mM, respectively, at pH 7.5 and 30 °C. The millimolar K_m value was of the same order as that for PP2Cα at pH 7.0 and 25 °C (*24*).

rWip1 Prefers a Diphosphorylated Substrate with a pTXpY Sequence. To clarify the substrate specificity of rWip1, we first examined the effect of a phosphorylated motif on substrate recognition. The kinetic parameters for a diphosphorylated p38α(180pT 182pY) peptide and a monophosphorylated p38α(180pT) peptide were measured at a constant Mg^{2+} concentration (Figure 2B). Estimated k_{cat} and K_m for the diphosphorylated p38α(180pT 182pY) peptide were higher and lower, respectively, than those of the monophosphorylated p38α(180pT) peptide (Table 1). The substrate specificity constant k_{cat}/K_m for the p38α(180pT 182pY) peptide was more than 5.5-fold higher than that of the p38α-(180pT) peptide (Table 1). In contrast, the monophosphorylated peptide was a better substrate for PP2Cα than the diphosphorylated peptide (Table 2). These results indicate that rWip1 shows a preference for diphosphorylated sequences and that the optimal substrate preference of Wip1 differs from that of PP2Cα.

To gain more information about the substrate specificity of rWip1, several phosphopeptides corresponding to the dephosphorylated site of p38α and UNG2 were analyzed (Table 1). Results using UNG2 phosphopeptides also showed that the diphosphorylated peptides were much better substrates than monophosphorylated peptides. There are two pTXpY sequences in UNG2 that become phosphorylated in response to DNA damage, but in vivo Wip1 dephosphorylates UNG2 at phosphothreonine 6 and not at phosphothreonine 126 (*16*). As expected, the diphosphorylated UNG2(6pT 8pY) peptide that has the phosphothreonine 6 of UNG2 was a better substrate than the diphosphorylated UNG2(126pT 128pY) peptide (Table 1). The diphosphorylated UNG2(6pT 8pY) peptide was a slightly better substrate for rWip1 than the diphosphorylated p38α (180pT 182pY) peptide (1.4-fold higher k_{cat}/K_m). Monophosphorylated UNG2(126pT) peptide was not dephosphorylated by rWip1 while activity was observed with monophosphorylated peptides p38α(180pT) and UNG2(6pT) (Table 1), suggesting that the proline residues that follow 126pT in UNG2 may inhibit recognition of this site by Wip1. Detectable activity was not observed with the phosphotyrosine peptides p38α(182pY), UNG2-(8pY), and UNG2(128pY). As previously reported for the kinetic analysis of PP2Cα (*26*, *37*, *38*), the phosphothreonine peptide RRApTVA was a substrate for PP2Cα (Table 2). However, RRApTVA and other UNG2 monophosphothreonine peptides having pT-(A/D/G/N/P/Q/V/W)-(A/E/H/I/M/P/R/V) sequences were not dephosphorylated by rWip1 (Table 1 and ref *16*). Phosphoserine analogues of p38α peptides also were not dephosphorylated by rWip1 and PP2Cα (Tables 1 and 2), although p38α(180pS 182pY) has a diphosphorylated motif. To examine the sequence specificity of the diphosphorylated motif of rWip1, derivatives of the wild-type peptide containing either phosphoserine or aspartic acid in place of phosphotyrosine, p38α(180pT 182pS) and p38α(180pT 182D), were tested. The k_{cat}/K_m for these were decreased by 5−10-fold compared to the p38α-(180pT 182pY) wild-type peptide (Table 1). These results indicate that rWip1 recognizes the diphosphorylated pTXpY sequence and is a threonine-specific phosphatase.

As described above, the diphosphorylated peptides p38α-(180pT 182pY) and UNG2(6pT 8pY) are both good substrates for rWip1, although the only conserved sequence they have in common is the pTXpY motif. To study the effect of individual side chains before and after the pTXpY sequence, we tested p38α(175−185)(180pT 182pY) peptides in which individual amino acids were substituted with alanine (Table

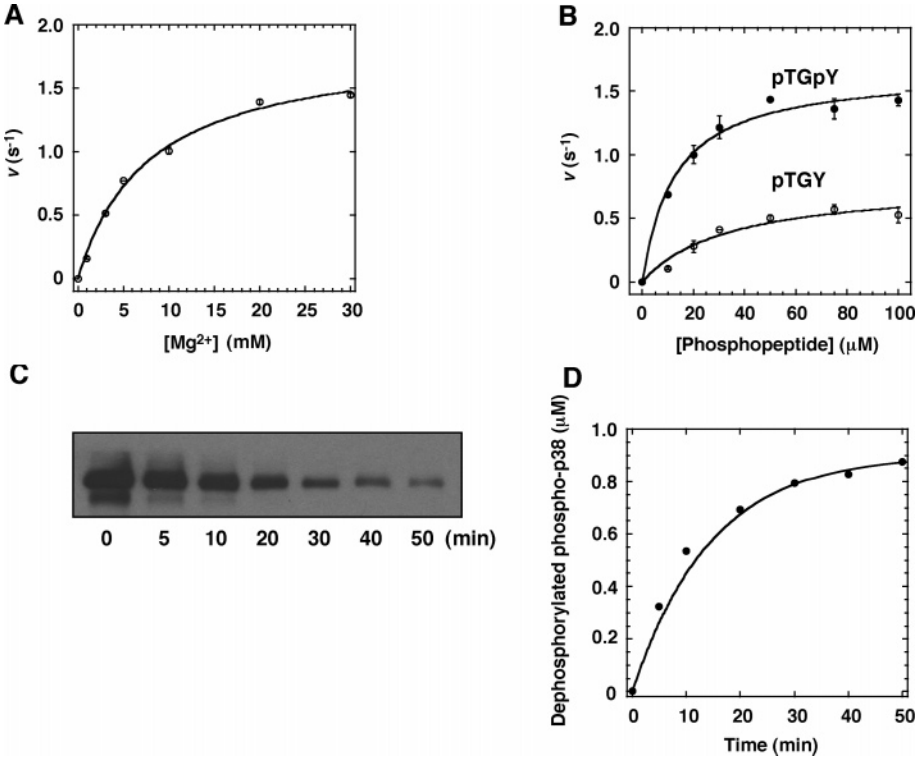

FIGURE 2: Kinetic analysis of rWip1. (A) Concentration dependence of Mg^{2+} on rWip1-catalyzed dephosphorylation of a p38α(175−185)(180pT 182pY) diphosphorylated peptide. The peptide concentration was 50 μM. (B) Concentration dependence of activity on the diphosphorylated (pTGpY) and the monophosphorylated (pTGY) p38α(175−185) peptide substrates. The concentration of Mg^{2+} was 30 mM. Phosphatase activity was measured by a malachite green/molybdate-based assay. The data in panels A and B were fitted to the Michaelis−Menten equation (eq 1) to estimate the kinetic parameters. The graph shows the mean ± standard error for at least three experiments. All assays were performed at 30 °C and pH 7.5. (C) Time-dependent dephosphorylation of the full-length p38α(180pT 182pY) GST-tagged phosphoprotein. rWip1 (0.4 μM) was incubated with GST-p38α phosphoprotein (1.0 μM) at 30 °C and pH 7.5 for 0−50 min. Dephosphorylation of the GST-p38α phosphoprotein was determined by immunoblotting analysis using anti-phospho-p38 antibody that did not recognize the nonphosphorylated GST-p38α protein (data not shown). The GST-p38α protein level in each reaction was confirmed with Coomassie staining (data not shown). (D) The data were fitted to the integrated Michaelis−Menten equation (eq 2) as described in the Experimental Procedures. The graph represents an average of two separate experiments.

Table 1: Kinetic Parameters for the Dephosphorylation of Synthetic Phosphopeptides by rWip1 at pH 7.5 and 30 °C[a]

substrate	sequence[b]	K_m (μM)	k_{cat} (s^{-1})	k_{cat}/K_m ($\times 10^3$ M^{-1} s^{-1})
p38α(180pT 182pY)	TDDEM**pT**G**pY**VAT	13 ± 2	1.7 ± 0.1	131
p38α(180pT)	TDDEM**pT**GYVAT	34 ± 12	0.8 ± 0.1	24
p38α(182pY)	TDDEMTG**pY**VAT	ND[c]	ND[c]	ND[c]
p38α(180pS 182pY)	TDDEM**pS**G**pY**VAT	ND[c]	ND[c]	ND[c]
p38α(180pS)	TDDEM**pS**GYVAT	ND[c]	ND[c]	ND[c]
p38α(180pT 182pS)	TDDEM**pT**G**pS**VAT	53 ± 11	0.7 ± 0.1	13
p38α(180pT 182D)	TDDEM**pT**GDVAT	52 ± 2	1.3 ± 0.03	25
UNG2(6pT 8pY)	MIGQK**pT**L**pY**SFF	9 ± 2	1.7 ± 0.1	189
UNG2(6pT)	MIGQK**pT**LYSFF	70 ± 11	1.6 ± 0.1	23
UNG2(8pY)	MIGQKTL**pY**SFF	ND[c]	ND[c]	ND[c]
UNG2(126pT 128pY)	ERKHY**pT**V**pY**PPPH	18 ± 6	0.9 ± 0.1	50
UNG2(126pT)	ERKHY**pT**VYPPPH	ND[c]	ND[c]	ND[c]
UNG2(128pY)	ERKHYTV**pY**PPPH	ND[c]	ND[c]	ND[c]
pThr peptide	RRA**pT**VA	ND[c]	ND[c]	ND[c]
ERK5(218pT 220pY)	HQYFM**pT**E**pY**VATR	36 ± 5	2.4 ± 0.1	67
JNK1(183pT 185pY)	TSFMM**pT**P**pY**VVTR	ND[c]	ND[c]	ND[c]

[a] Values represent averages from two to four independent experiments. [b] Phosphorylated amino acids are indicated in bold type. [c] The K_m and k_{cat} values could not be determined due to the high K_m.

3). The largest effect of alanine substitution was at position −3 (D177A), which decreased k_{cat}/K_m by 2.5-fold. Peptides with alanine substituted for the residues before and after the pTGpY sequence (M179A and V183A, respectively) were slightly poorer substrates for rWip1 than the wild-type peptide. A p38α peptide with alanine substituted for glycine between the phosphothreonine and phosphotyrosine (G181A) decreased the K_m 1.6-fold to a value (8 μM) similar to that of the UNG2(6pT 8pY) peptide that has leucine between the phosphorylated residues. However, the differences in kinetic parameters between the wild-type peptide and alanine-scan peptides (Table 3) were much smaller than the differences between di- and monophosphorylated peptides (Table 1).

Table 2: Kinetic Parameters for the Dephosphorylation of Synthetic Phosphopeptides by Recombinant Human PP2Cα at pH 7.5 and 30 °C[a]

substrate	sequence[b]	K_m (μM)	k_{cat} (s^{-1})	k_{cat}/K_m ($\times 10^3$ M^{-1} s^{-1})
p38α(180pT 182pY)	TDDEM**pT**G**pY**VAT	63 ± 5	2.8 ± 0.1	44
p38α(180pT)	TDDEM**pT**GYVAT	44 ± 4	3.4 ± 0.2	77
p38α(180pS 182pY)	TDDEM**pS**G**pY**VAT	ND[c]	ND[c]	ND[c]
p38α(180pS)	TDDEM**pS**GYVAT	ND[c]	ND[c]	ND[c]
pThr peptide	RRA**pT**VA	57 ± 3	4.1 ± 0.1	72

[a] Values are averages from two to three independent experiments. [b] Phosphorylated amino acids are indicated in bold type. [c] The K_m and k_{cat} values could not be determined due to the high K_m.

Table 3: Kinetic Parameters for the Dephosphorylation of p38α(175−185)(180pT 182pY) Alanine-Scan Peptides by rWip1 at pH 7.5 and 30 °C[a]

substrate	sequence[b]	K_m (μM)	k_{cat} (s^{-1})	k_{cat}/K_m ($\times 10^3$ M^{-1} s^{-1})
p38α(180pT 182pY)	TDDEMpTGpYVAT	13 ± 2	1.7 ± 0.1	131
T175A	**A**DDEMpTGpYVAT	11 ± 1	1.3 ± 0.03	118
D176A	T**A**DEMpTGpYVAT	13 ± 3	1.6 ± 0.1	123
D177A	TD**A**EMpTGpYVAT	30 ± 4	1.6 ± 0.1	53
E178A	TDD**A**MpTGpYVAT	15 ± 2	1.9 ± 0.1	127
M179A	TDDE**A**pTGpYVAT	20 ± 4	1.5 ± 0.1	75
G181A	TDDEMpT**A**pYVAT	8 ± 1	1.6 ± 0.04	200
V183A	TDDEMpTGpY**A**AT	20 ± 5	1.1 ± 0.1	55
T185A	TDDEMpTGpYVA**A**	11 ± 2	1.2 ± 0.04	109

[a] Values are averages from two to four independent experiments. [b] The replaced alanine residues are indicated in bold type.

Table 4: Kinetic Parameters for the Dephosphorylation of UNG2 Short Phosphopeptides by rWip1 at pH 7.5 and 30 °C[a]

substrate	sequence[b]	K_m (μM)	k_{cat} (s^{-1})	k_{cat}/K_m ($\times 10^3$ M^{-1} s^{-1})
UNG2(6−8)(6pT 8pY)	**pT**L**pY**-NH_2	ND[c]	ND[c]	ND[c]
UNG2(5−9)(6pT 8pY)	K**pT**L**pY**S-NH_2	20 ± 2	0.8 ± 0.03	40
UNG2Ac-(5−9)(6pT 8pY)	Ac-K**pT**L**pY**S-NH_2	19 ± 1	1.5 ± 0.03	79

[a] Values are averages from four independent experiments. [b] Phosphorylated amino acids are indicated in bold type. An acetylation of the N-terminus and amidation of the C-terminus are denoted by Ac- and -NH_2, respectively. [c] The K_m and k_{cat} values could not be determined due to the high K_m.

rWip1 Recognizes Different Chain-Length Peptides as Substrates. To evaluate the effect of chain length on substrate specificity of rWip1, short chain length analogues of the UNG2(6pT 8pY) peptide were assayed (Table 4). Diphosphorylated UNG2(6−8)(6pT 8pY), a three-residue peptide having only the pTLpY sequence, was not dephosphorylated by rWip1. However, adding only one residue to both the N- and C-termini, which created a five-residue peptide, produced a valid substrate. Acetylation at the N-terminus of the five-residue peptide increased the k_{cat} 1.9-fold but did not affect the K_m compared to the nonacetylated peptide. These results indicate that rWip1 recognizes substrates of different chain lengths, but they must be at least five residues in length and must include the pTXpY sequence.

The X Residue in the pTXpY Sequence Affects the Affinity for rWip1. As described above, UNG2(6pT 8pY) (-pTLpY-) and p38α(180pT 182pY)(G181A) (-pTApY-) peptides exhibited approximately a 1.5-fold lower K_m than p38α(180pT 182pY) (-pTGpY-), although the k_{cat} of these three peptides were very similar. These data suggested that the residue (X) between phosphothreonine and phosphotyrosine may affect the substrate's affinity for rWip1. Extracellular signal-regulated kinases (ERKs), which belong to the MAPK family, have a pTEpY sequence. We therefore measured the kinetic parameters for a human ERK5(213−224)(218pT 220pY) diphosphorylated peptide, although it has not been reported that ERK5 is a substrate for Wip1 in vivo. As shown in Table 1, the k_{cat} for this peptide increased 1.4-fold, and the K_m was 2.8-fold higher than for the p38α(180pT 182pY) peptide. As a result, the k_{cat}/K_m for the ERK5 peptide is 2.0-fold smaller than for the p38α peptide. Furthermore, a diphosphorylated human JNK1(178−189)(183pT 185pY) peptide (Table 1) and the phosphorylated JNK MAPK protein (*12*), which have the sequence pTPpY, were not Wip1 substrates, suggesting that a proline at the X position is incompatible with substrate recognition. These results indicate that the X residue in the pTXpY sequence modulates the affinity for rWip1 and determines selectivity toward different MAPKs.

The Full-Length p38 Phosphoprotein Is an Efficient Substrate for rWip1. To examine further the requirements for substrate recognition by rWip1, k_{cat}/K_m for the full-length p38α phosphoprotein was measured. Dephosphorylation was detected by immunoblot analysis using an antibody that specifically recognizes the diphosphorylated form of the p38α protein (Figure 2C). The bands were quantified by densitometry, and the data were fitted to the integrated Michaelis−Menten equation (eq 2) (Figure 2D). The estimated k_{cat}/K_m value for the full-length p38α phosphoprotein was 1.6×10^6 M^{-1} s^{-1}. This value is about 12-fold higher than that for the diphosphorylated p38α peptide (Table 1). This result suggested that regions or motifs outside the pTXpY sequence contribute to substrate recognition by rWip1 either directly or through effects on the conformation of the phosphorylated segment.

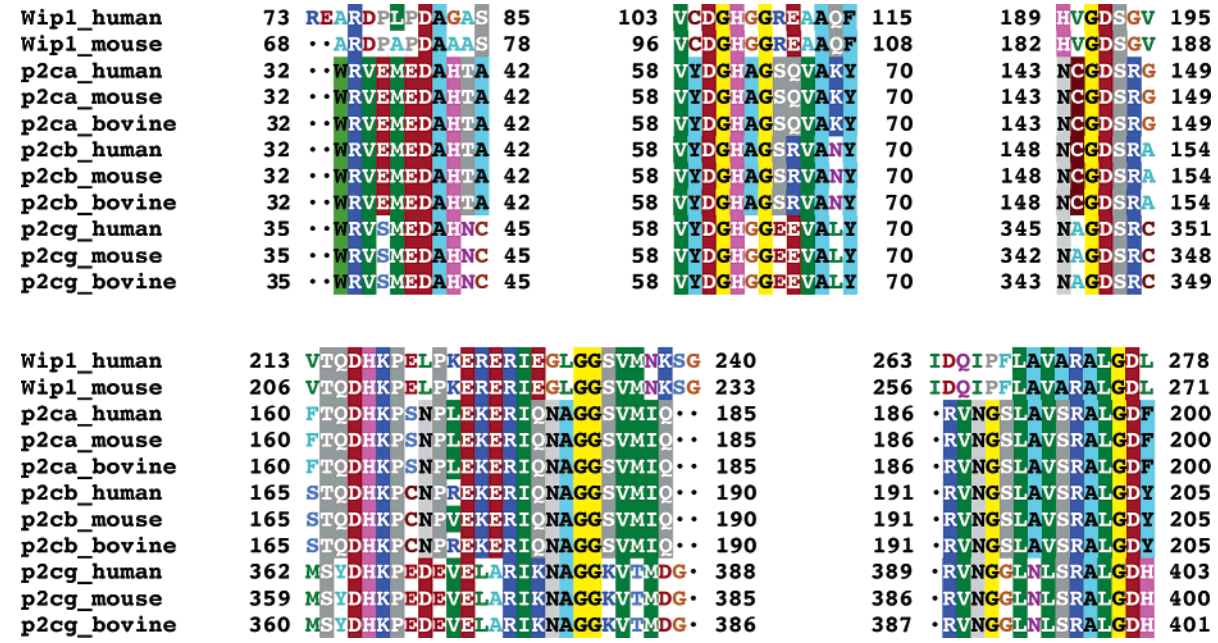

FIGURE 3: Sequence alignment of mammalian members of the PP2C family: α, *β*, *γ*, and *δ* (Wip1) subfamilies. The illustration has been reduced in both number of sequences and positions for clarity and to highlight the enzymatic catalytic site. The "p2c(a,b,g)" prefixes of the sequence names are the Swiss-Prot Protein Knowledgebase (*29*) designations for the α, *β*, and *γ* subfamilies.

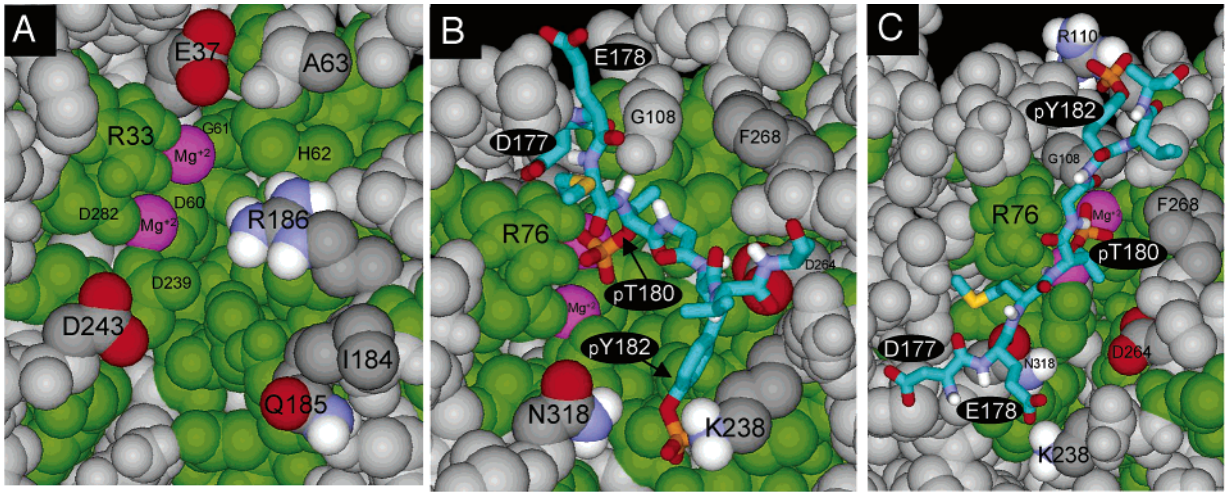

FIGURE 4: Comparison of the catalytic site structures of PP2Cα (*32*) and the Wip1 homology model. Residues outside of the active site are colored light gray. Identical catalytic site residues for the two enzymes are colored green. Active site residue side chains that differ are color-coded by atom type (carbon, dark gray; nitrogen, blue; oxygen, red; hydrogen, white). The two magnesium ions are colored magenta. (A) Crystal structure of PP2Cα [1A6Q.pdb; Protein Data Bank (*44*)]. (B) Primary mode of binding of the p38 peptide, DEMpTGpYVA, in the active site of Wip1. For clarity, a single peptide is shown rather than the full population of docked substrate molecules. In addition to the color codes for N, O, and H given above, the peptide carbons are colored teal, the phosphates are colored orange, and the sulfurs are colored yellow. The labels of the peptide residues are distinguished by black oval backgrounds. (C) Secondary mode of binding of the p38 peptide to Wip1.

Structural Analysis. To investigate the physicochemical, molecular basis for the observed substrate specificities, a homology model of human Wip1 was developed from the crystal structure of PP2Cα (*32*). This required first updating the multiple sequence alignments we have previously published for the PP2C family (*10*, *39*) by concentrating only on the α, *β*, *γ*, and *δ* subfamilies of animal species. Special consideration was given to the sequence regions comprising the catalytic site, favoring alignments conserving specific residues suggested to be structurally and functionally important from analysis of the crystal structure template (*32*, *40*). For example, as seen in Figure 3, R76 of human Wip1 (conserved as R69 in mouse Wip1) is aligned with the active site R33 of PP2Cα, despite the lack of sequence identity of the immediately flanking residues between Wip1 and the other members. The guanidinium group of the arginine residue is often found in the catalytic site of phosphatases, such as tyrosine phosphatases or PP2B serine/threonine phosphatase, and interacts with a phosphate on the substrate (*41*). A mutagenesis study of PP2Cα confirmed that R33 is an important residue for substrate affinity (*40*). For the most part, there is a high degree of conservation among all of the sequences of the residues forming the active site. In addition to Figure 3, this is demonstrated structurally in Figure 4A, where all of the metal-binding and directly adjacent residues are identical between Wip1 and PP2Cα and only a minority of residues on the periphery differ (i.e., E37, A63, I184, Q185, R186, and D243 of human PP2Cα). This agrees with

the finding that rWip1 has a similar affinity for Mg^{2+} compared to PP2Cα (Figure 2A). Clues for understanding specificity differences are obtained from the alignment depicted in Figure 3, which points out catalytic site positions that are conserved within but differ between two or more PP2C subfamilies. Among these, variations that are the least conservative in size, polarity, and/or formal electrostatic charge are likely to be more influential. For PP2Cα vs Wip1 these are E37/P80, Q185/K238, R186/D264, and D243/N318.

The next step was to compare computer simulations of the p38 peptide substrate binding to the PP2Cα and Wip1 catalytic sites and correlate these with the experimental kinetic results. While not identifying any single complex as uniquely preferred, this comparison produced a sample of the range of possible energetically stabilized structures, which was then clustered into different modes of binding. The most dominant mode (i.e., the most highly populated) of the p38 diphosphorylated peptide substrate binding to Wip1 is shown in Figure 4B. This structure is characterized by the phosphate of the threonine (pT180 of p38) remaining bound to the catalytic site R76 residue and the phosphate of the tyrosine (pY182 of p38) bound to the positively charged K238 side chain. In addition, it is seen that the p38 D177 residue forms a stabilizing salt-bridge interaction with the active site R76 residue, whereas the adjacent E178 residue simply extends into the solvent. Figure 4C shows a second, less populated mode for the interaction of the diphosphorylated p38 peptide binding with Wip1. In this case, the substrate backbone is rotated 180° around the phosphothreonine, allowing the phosphotyrosine to make a salt bridge with R110, which is slightly beyond what we conservatively estimated to be part of the substrate-binding region. As seen in Figure 3, R110 is another position that is conserved within the PP2C family but differs between PP2Cα and Wip1: i.e., S65/R110. As also seen in Figure 4C, contrary to the primary binding mode, the p38 E178 residue, rather than D177, formed a salt bridge with K238; however, this association was not consistent throughout the population, and D177 also formed a salt bridge with K238 with equal frequency in this binding mode.

Lysine 238 of rWip1 Is Important for Binding the Phosphotyrosine in the pTXpY Sequence. To investigate the roles of residues K238 and R110 in substrate recognition, the kinetic parameters for rWip1 single amino acid mutants were measured using the wild-type p38α diphosphorylated peptide. K238 was changed by mutation to glutamine or aspartic acid, and R110 was changed to serine or glutamic acid, all of which are conserved in at least one of the α, *β*, and/or *γ* subfamily sequences (Figure 3). Mutant proteins with the K238Q, K238D, or R110E changes were expressed in soluble form by coexpression with chaperone proteins (see Experimental Procedures); however, rWip1 with R110S was not expressed under these expression conditions. The three soluble, mutant rWip1 proteins showed the same property of threonine-specific dephosphorylation as wild-type rWip1 (data not shown).

As seen in Tables 1 and 5, the K238Q and K238D mutations resulted in elevated K_m values compared with wild-type rWip1 for both the monophosphorylated p38α(180pT) and diphosphorylated p38α(180pT 182pY) peptides. The ratio of values for mono- over diphosphorylated peptides, which indicates the relative preference for the diphosphorylated substrate, was 2.6 for wild-type rWip1 and decreased to 1.6 and 1.1 for the mutant proteins, respectively. In contrast, the R110E mutant showed similar K_m values for both the mono- and diphosphorylated peptides as the wild-type rWip1. However, in this case, the k_{cat} values increased approximately 3- and 2-fold for the two substrates. The changes K238Q and K238D also caused a progressive decrease in the k_{cat}/K_m values compared with the wild-type enzyme for both the mono- and diphosphorylated substrates, with the change being larger for the latter one. Since the R110E mutant and wild-type rWip1 proteins had similar K_m values, the change in the k_{cat}/K_m for this mutant reflected the same 3- and 2-fold increase as the k_{cat} values just described. The ratio of k_{cat}/K_m values for the di- over monophosphorylated substrates, which indicates the selectivity preference due to the phosphotyrosine, changed from 5.5 for the wild-type rWip1 to 2.4 for the K238Q mutant, 1.9 for the K238D mutant, and 3.5 for the R110E mutant proteins. These results suggest that K238 plays an important role in substrate discrimination by recognizing the phosphotyrosine in the pTXpY motif, as suggested by molecular modeling.

Table 5: Kinetic Parameters for the Dephosphorylation of p38α Phosphopeptides by rWip1 Mutants at pH 7.5 and 30 °C[a]

mutant	substrate[b]	K_m (μM)	k_{cat} (s^{-1})	k_{cat}/K_m ($\times 10^3$ M^{-1} s^{-1})
K238Q	TDDEM**pT**G**pY**VAT	34 ± 5	1.3 ± 0.1	38
	TDDEM**pT**GYVAT	56 ± 9	0.9 ± 0.1	16
K238D	TDDEM**pT**G**pY**VAT	39 ± 3	0.9 ± 0.03	23
	TDDEM**pT**GYVAT	43 ± 3	0.5 ± 0.2	12
R110E	TDDEM**pT**G**pY**VAT	13 ± 0.9	3.4 ± 0.6	262
	TDDEM**pT**GYVAT	39 ± 4	2.9± 0.1	74

[a] Values are averages from two to three independent experiments. [b] Phosphorylated amino acids are indicated in bold type.

DISCUSSION

Identification of physiological substrates for protein phosphatases is important for understanding their biological mechanisms. It had previously been reported that p38 MAPK and UNG2 are physiological targets of Wip1 (*12*, *16*); however, *PPM1D* null mice exhibit defects in reproductive organs, immune function, and cell cycle control (*23*), suggesting that there must be other physiological targets of Wip1. In this study, we investigated the substrate specificity of Wip1 by kinetic analysis using recombinant Wip1 (amino acids 1−420 of the human enzyme) and various phosphopeptides.

Optimal Substrate Sequence. On the basis of the present results, we propose that the optimal substrate sequence for Wip1 may be X_{-1}-pT-X_{+1}-pY-X_{+3}, where X_{-1}, X_{+1}, and X_{+3} denote any amino acid, any aliphatic amino acid, and any amino acid except proline, respectively. This optimal sequence clearly is consistent with the findings that the MKK1, MKK4, and MKK6 MAPKKs, which have the pSXXX(pS/pT) sequence, or JNK1 and ERK2 MAPKs, which have the pT(P/E)pY sequence, are not physiological substrates for Wip1 as reported previously (*12*). Furthermore, the X residue between the phosphothreonine and phosphotyrosine residues in the pTXpY sequence modulated the affinity of peptides for Wip1. These findings suggest that Wip1 recognizes a very narrow region around the pTXpY sequence and this

core region may be important for the binding of corresponding substrate peptides and for the catalytic activity of Wip1.

Although both Wip1 and PP2Cα dephosphorylated the threonine residue of the pTGpY sequence in p38 MAPK in vivo and in vitro (*5*, *12*), other reported substrates of PP2Cα are different from those preferred by Wip1. Previous kinetic studies showed that the monophosphorylated peptides RRApTVA (*26*, *37*) or FLRpTSCG and FLRTpTCG, derived from AMPK (*38*), are good substrates for PP2Cα. In accord with those studies, our kinetic results also showed that the monophosphorylated peptides are better substrates for PP2Cα than diphosphorylated peptides (Table 2). Moreover, PP2Cα can bind and dephosphorylate the serine residues of the (R/K)XpS sequences on CFTR (*42*) and metabotropic glutamate receptor 3 (*43*) in vivo and/or in vitro. These results indicated that the optimal substrate sequences of Wip1 and PP2Cα are different and that Wip1 has much narrower substrate specificity than PP2Cα.

Structural Analysis. The computer simulations predicted that the most likely mode of p38α(180pT 182pY) peptide binding has the phosphate of the tyrosine forming a salt bridge with the K238 residue of the rWip1 enzyme (Figure 4B). This is consistent with the pattern of sequence conservation seen in the alignment of Figure 3, in which a positively charged residue at this position occurs only in the diphosphorylated-selective, Wip1 subfamily. Experimental evidence that this energetically stabilizing salt bridge is responsible for the enhanced preference of Wip1 for diphosphorylated, pTXpY-containing substrates (Tables 1 and 2) comes from comparison of the kinetic parameters of the wild type and three single amino acid substituted rWip1 enzymes (Tables 1 and 5). Specifically, the K238Q and K238D derivatives resulted in a progressive reduction in preference of the di- vs monophosphorylated substrate compared to the wild-type protein (Tables 1 and 5). The larger decrease for the latter mutation can be understood by the added electrostatic repulsion of the negatively charged phosphotyrosine upon changing from net-neutral glutamine to the negatively charged aspartic acid. Likewise, the enhanced diphosphorylated selectivity of the R110E mutant over the K238 mutants could be explained by electrostatic repulsion with the negatively charged glutamic acid, which might reduce the population of peptides in the secondary binding mode (Figure 4C), thus increasing the population in the catalytic binding mode (Figure 4B). A possible contradiction to this hypothesis is that simulations with PP2Cα as the target had the phosphotyrosine forming an alternative salt bridge with the positively charged R148 residue. As seen in Figure 3, this residue is conserved in all α, *β*, and *γ* subfamilies but is glycine in Wip1. However, because of the closer distance to the phosphothreonine, the substrate peptide bound to PP2Cα must form a tight hairpin structure that protrudes into the solution, thus preventing other stabilizing interactions with the enzyme. In contrast, the K238 residue in Wip1 is ideally placed to allow the backbone of the substrate to assume an extended conformation that interacts with other residues at the bottom and/or sides of the extended catalytic site. As also described above, the fact that the p38 D177 residue makes a stabilizing salt bridge and E178 does not (Figure 4B) is consistent with the alanine-scanning results in Table 3 that the former residue influences both binding and specificity and that the latter is relatively uninvolved.

Unfortunately, the resolution of the numerical simulations was not sufficient to investigate more subtle attributes of the substrate. For example, analyses of the type of side chain between the phosphorylated residues of the pTXpY motif, or the minor structural difference from substituting phosphoserine for phosphothreonine, which caused a relatively large reduction in the kinetics as presented in Table 1 and reported by others (*26*, *37*, *38*), were not informative. Such detail would likely require more accurate energy functions that better account for the entropy and solvent effects in the former case and the effects of differences in molecular orbitals on the dynamic catalytic reaction for the latter.

In conclusion, our results show that peptides which contain the pTXpY motif are the optimal substrates for Wip1 and that the motif present in the amino acid sequence of these peptides dictates selectivity for both in vivo and in vitro substrates. Knowing that the pTXpY motif in two substrates, p38 and UNG2, is important for substrate recognition should facilitate the recognition of other important unknown substrates. Recent studies have shown that inhibiting Wip1 activity may suppress the proliferation of certain types of cancer cells (*21*, *22*). Therefore, our results should be useful for designing and synthesizing novel anticancer drugs.

REFERENCES

1. Barford, D. (1996) Molecular mechanisms of the protein serine/threonine phosphatases, *Trends Biochem. Sci. 21*, 407−412.
2. Ingebritsen, T. S., and Cohen, P. (1983) Protein phosphatases: properties and role in cellular regulation, *Science 221*, 331−338.
3. Cohen, P., Holmes, C. F. B., and Tsukitani, Y. (1990) Okadaic acid: a new probe for the study of cellular regulation, *Trends Biochem. Sci. 15*, 98−102.
4. Lewis, T. S., Shapiro P. S., and Ahn, N. G. (1998) Signal transduction through MAP kinase cascades, *Adv. Cancer Res. 74*, 49−139.
5. Takekawa, M., Maeda, T., and Saito, H. (1998) Protein phosphatase 2Cα inhibits the human stress-responsive p38 and JNK MAPK pathways, *EMBO J. 17*, 4744−4752.
6. Hanada, M., Kobayashi, T., Ohnishi, M., Ikeda, S., Wang, H., Katsura, K., Yanagawa, Y., Hiraga, A., Kanamaru, R., and Tamura, S. (1998) Selective suppression of stress-activated protein kinase pathway by protein phosphatase 2C in mammalian cells, *FEBS Lett. 437*, 172−176.
7. Maeda, T., Wurgler-Murphy, S. M., and Saito, H. (1994) A two-component system that regulates an osmosensing MAP kinase cascade in yeast, *Nature 369*, 242−245.
8. Nguyen, A. N., and Shiozaki, K. (1999) Heat-shock-induced activation of stress MAP kinase is regulated by threonine- and tyrosine-specific phosphatases, *Gene Dev. 13*, 1653−1663.
9. Warmka, J., Hanneman, J., Lee, J., Amin, D., and Ota, I. (2001) Ptc1, a type 2C Ser/Thr phosphatase, inactivates the HOG pathway by dephosphorylating the mitogen-activated protein kinase Hog1, *Mol. Cell. Biol. 21*, 51−60.
10. Meskiene, I., Baudouin, E., Schweighofer, A., Liwosz, A., Jonak, C., Rodriguez, P. L., Jelinek, H., and Hirt, H. (2003) Stress-induced protein phosphatase 2C is a negative regulator of a mitogen-activated protein kinase, *J. Biol. Chem. 278*, 18945−18952.
11. Fiscella, M., Zhang, H., Fan, S., Sakaguchi, K., Shen, S., Mercer, W. E., Vande Woude, G. F., O'Connor, P. M., and Appella, E. (1997) Wip1, a novel human protein phosphatase that is induced in response to ionizing radiation in a p53-dependent manner, *Proc. Natl. Acad. Sci. U.S.A. 94*, 6048−6053.
12. Takekawa, M., Adachi, M., Nakahata, A., Nakayama, I., Itoh, F., Tsukuda, H., Taya, Y., and Imai, K. (2000) p53-inducible wip1 phosphatase mediates a negative feedback regulation of p38 MAPK-p53 signaling in response to UV radiation, *EMBO J. 19*, 6517−6526.
13. Sanchez-Prieto, R., Rojas, J. M., Taya, Y., and Gutkind, J. S. (2000) A role for the p38 mitogen-acitvated protein kinase

pathway in the transcriptional activation of p53 on genotoxic stress by chemotherapeutic agents, *Cancer Res. 60*, 2464−2472.
14. Bulavin, D. V., Saito, S., Hollander, M. C., Sakaguchi, K., Anderson, C. W., Appella, E., and Fornace, A. J., Jr. (1999) Phosphorylation of human p53 by p38 kinase coordinates N-terminal phosphorylation and apoptosis in response to UV radiation, *EMBO J. 18*, 6845−6854.
15. Kishi, H., Nakagawa, K., Matsumoto, M., Suga, M., Ando, M., Taya, Y., and Yamaizumi, M. (2001) Osmotic shock induces G1 arrest through p53 phosphorylation at Ser33 by activated p38MAPK without phosphorylation at Ser15 and Ser20, *J. Biol. Chem. 276*, 39115−39122.
16. Lu, X., Bocangel, D., Nannenga, B., Yamaguchi, H., Appella, E., and Donehower, L. A. (2004) The p53-induced oncogenic phosphatase PPM1D interacts with uracil DNA glycosylase and suppresses base excision repair, *Mol. Cell 15*, 621−634.
17. Li, J., Yang, Y., Peng, Y., Austin, R. J., van Eyndhoven, W. G., Nguyen, K. C., Gabriele, T., McCurrach, M. E., Marks, J. R., Hoey, T., Lowe, S. W., and Powers, S. (2002) Oncogenic properties of PPM1D located within a breast cancer amplification epicenter at 17q23, *Nat. Genet. 31*, 133−144.
18. Bulavin, D. V., Demidov, O. N., Saito, S., Kauraniemi, P., Phillips, C., Amundson, S. A., Ambrosino, C., Sauter, G., Nebreda, A. R., Anderson, C. W., Kallioniemi, A., Fornace, A. J., Jr., and Appella, E. (2002) Amplification of *PPM1D* in human tumors abrogates p53 tumor-suppressor activity, *Nat. Genet. 31*, 210−215.
19. Saito-Ohara, F., Imoto, I., Inoue, J., Hosoi, H., Nakagawara, A., Sugimoto, T., and Inazawa, J. (2003) PPM1D is a potential target for 17q gain in neuroblastoma, *Cancer Res. 63*, 1876−1883.
20. Hirasawa, A., Saito-Ohara, F., Inoue, J., Aoki, D., Susumu, N., Yokoyama, T., Nozawa, S., Inazawa, J., and Imoto, I. (2003) Association of 17q21-q24 gain in ovarian clear cell adenocarcinomas with poor prognosis and identification of PPM1D and APPBP2 as likely amplification targets, *Clin. Cancer Res. 9*, 1995−2004.
21. Bulavin D. V., Phillips, C., Nannenga, B., Timofeev, O., Donehower, L. A., Anderson, C. W., Appella, E., and Fornace, A. J., Jr. (2004) Inactivation of the Wip1 phosphatase inhibits mammary tumorigenesis through p38 MAPK-mediated activation of the $p16^{Ink4a}$-$p19^{Arf}$ pathway, *Nat. Genet. 36*, 343−350.
22. Bernards, R. (2004) Wip-ing out cancer, *Nat. Genet. 36*, 319−320.
23. Choi, J., Nannenga, B., Demidov, O. N., Bulavin, D. V., Cooney, A., Brayton, C., Zhang, Y., Mbawuike, I. N., Bradley, A., Appella, E., and Donehower, L. A. (2002) Mice deficient for the wild-type p53-induced phosphatase gene (*Wip1*) exhibit defects in reproductive organs, immune function, and cell cycle control, *Mol. Cell. Biol. 22*, 1094−1105.
24. Fjeld, C. C., and Denu, J. M. (1999) Kinetic analysis of human serine/threonine protein phosphatase 2Cα, *J. Biol. Chem. 274*, 20336−20343.
25. Harder, K. W., Owen, P., Wong, L. K. H., Aebersold, R., Clark-Lewis, I., and Jirik, F. R. (1994) Characterization and kinetic analysis of the intracellular domain of human protein tyrosine phosphatase β (HPTP β) using synthetic phosphopeptides, *Biochem. J. 298*, 395−401.
26. Donella-Deana, A., Boschetti, M., and Pinna, L. A. (2003) Monitoring of PP2A and PP2C by phosphothreonyl peptide substrates, *Methods Enzymol. 366*, 3−17.
27. Zhang, Z. Y., Maclean, D., Thieme-Sefler, A. M., Roeske, R. W., and Dixon, J. E. (1993) A Continuous spectrophotometric and fluorimetric assay for protein tyrosine phosphatase using phosphotyrosine-containing peptides, *Anal. Biochem. 211*, 7−15.
28. Kim, Y., Rice, A. E., and Denu, J. M. (2003) Intramolecular dephosphorylation of ERK by MKP3, *Biochemistry 42*, 15197−15207.
29. Apweiler, R., Bairoch, A., Wu, C. H., Barker, W. C., Boeckmann, B., Ferro, S., Gasteiger, E., Huang, H., Lopez, R., Magrane, M., Martin, M. J., Natale, D. A., O'Donovan, C., Redaschi, N., and Yeh, L. S. (2004) UniProt: the Universal Protein Knowledgebase, *Nucleic Acids Res. 32*, D115−D119.
30. Thompson, J. D., Gibson, T. J., Plewniak, F., Jeanmougin, F., and Higgins, D. G. (1997) The ClustalX windows interface: flexible strategies for multiple sequence alignment aided by quality analysis tools, *Nucleic Acids Res. 25*, 4876−4882.
31. Guex, N., and Peitsch, M. C. (1997) SWISS-MODEL and the Swiss-PdbViewer: An environment for comparative protein modeling, *Electrophoresis 18*, 2714−2723.
32. Das, A. K., Helps, N. R., Cohen, P. T., and Barford D. (1996) Crystal structure of the protein serine/threonine phosphatase 2C at 2.0 Å resolution, *EMBO J. 15*, 6798−6809.
33. Morris, G. M., Goodsell, D. S., Halliday, R. S., Huey, R., Hart, W. E., Belew, R. K., and Olson, A. J. (1998) Automated docking using a Lamarckian genetic algorithm and empirical binding free energy function, *J. Comput. Chem. 19*, 1639−1662.
34. Brooks, B. R., Bruccoleri, R. E., Olafson, B. D., States, D. J., Swaminathan, S., and Karplus, M. (1983) CHARMM: A program for macromolecular energy, minimization, and dynamics calculations, *J. Comput. Chem. 4*, 187−217.
35. Cohen, P. (1989) The structure and regulation of protein phosphatases, *Annu. Rev. Biochem. 58*, 453−508.
36. Yamashita, K., Yasuda, H., Pines, J., Yasumoto, K., Nishitani, H., Ohtsubo, M., Hunter, T., Sugimura, T., and Nishimoto T. (1990) Okadaic acid, a potent inhibitor of type 1 and type 2A protein phosphatases, activates cdc2/H1 kinase and transiently induces a premature mitosis-like state in BHK21 cells, *EMBO J. 13*, 4331−4338.
37. Pinna, L. A., and Donella-Deana, A. (1994) Phosphorylated synthetic peptides as tools for studying protein phosphatases, *Biochim. Biophys. Acta 1222*, 415−431.
38. Marley, A. E., Sullivan, J. E., Carling, D., Abbott, W. M., Smith, G. J., Taylor, I. W. F., Carey, F., and Beri, R. K. (1996) Biochemical characterization and deletion analysis of recombinant human protein phosphatase 2Cα, *Biochem. J. 320*, 801−806.
39. Choi, J., Appella, E., and Donehower, L. A. (2000) The structure and expression of the murine wild-yype p53-induced phosphatase 1 (*Wip1*) gene, *Genomics 64*, 298−306.
40. Jackson, M. D., Fjeld, C. C., and Denu, J. M. (2003) Probing the function of conserved residues in the serine/threonine phosphatase PP2Cα, *Biochemistry 42*, 8513−8521.
41. Jackson, M. D., and Denu, J. M. (2001) Molecular reactions of protein phosphatases-insights from structure and chemistry, *Chem. Rev. 101*, 2313−2340.
42. Travis, S. M., Berger, H. A., and Welsh, M. J. (1997) Protein phosphatase 2C dephosphorylates and inactivates cystic fibrosis transmembrane conductance regulator, *Proc. Natl. Acad. Sci. U.S.A. 94*, 11055−11060.
43. Flajolet, M., Rakhilin, S., Wang, H., Starkova, N., Nuangchamnong, N., Nairn, A. C., and Greengard, P. (2003) Protein phosphatase 2C binds selectively to and dephosphorylates metabotropic glutamate receptor 3, *Proc. Natl. Acad. Sci. U.S.A. 100*, 16006−16011.
44. Berman, H. M., Westbrook, J., Feng, Z., Gilliland, G., Bhat, T. N., Weissig, H., Shindyalov, I. N., and Bourne, P. E. (2000) The Protein Data Bank, *Nucleic Acids Res. 28*, 235−242.

BI0476634